Cellular and Molecular Biology
E-ISSN : 1165-158X / P-ISSN : 0145-5680
www.cellmolbiol.org

Diagnosis of breast cancer lesion using ultrasound images, elastography, and Ki-67 protein cell proliferation index

Yulin Fang, Yanjun Zhou*

Department of Ultrasound in Medicine, The Second Affiliated Hospital of Zhejiang University, Lanxi Branch (Lanxi People's Hospital),1359 Xishan Road, Lanxi, Zhejiang, China, 321100

ARTICLE INFO

Original paper

Article history:
Received: January 12, 2022
Accepted: April 01, 2023
Published: April 30, 2023

Keywords:

Elastography, ultrasound, Ki-67 protein, breast cancer

ABSTRACT

Today, using elastography and ultrasound images is the best method for diagnosing breast cancer for dense tissues, especially for women under 30 years old, which is used to detect the exact border of masses. Besides, using quantitative microscopic criteria that are less tasteful seems to be useful in predicting the behavior of the tumor and its prognosis. Ki-67 is an antigen corresponding to a nuclear non-histone protein produced by cells in proliferative phases. In this article, ultrasound and elastography images of patients were collected, and breast masses were identified. The proposed algorithm includes pre-processing, feature extraction, and classification. To remove the speckle noise, two pre-processing steps are used, and after segmenting each data with its appropriate color channel, statistical features and features based on the morphology of suspicious areas are extracted. Also, sections of paraffin blocks of samples fixed in formalin were prepared and stained by immunohistochemical staining with Ki-67 monoclonal antibody, and the cell proliferation index was determined in the prepared slides. The relationship between Ki-67 positivity and microscopic grade was studied. The feature extraction results show that elastography is chosen as a more appropriate method than ultrasound due to the separation in terms of color channels. The most appropriate proposed combined methods, namely RBF-Kmeans, MLP-SCG, and RBF-SOM, have been used to classify features. The combined MLP-SCG classifier with an average accuracy of 96% and an average of 98% has improved significantly compared to other methods.

Doi: http://dx.doi.org/10.14715/cmb/2023.69.4.3

Introduction

Breast cancer is the second most common cause of cancer death among women (1). The average age of patients is 49.6 years, which shows the severe need for early diagnosis (2). One of the most important types of applications of medical diagnosis systems is the identification of masses and their classification, which makes the amount of radiation attenuation by the desired mass density (3). There are various methods for diagnosing breast cancer, based on light, sound, heat, magnetism, attenuation, microwaves, X-rays, nuclear, electrical impedance, and computer modeling (inverse problem) or a combination of several methods and diagnoses (4). They are computer-aided. Magnetic resonance imaging (MRI), ultrasound imaging, thermography, and X-ray can be mentioned as imaging-based methods (5). In this article, two types of ultrasound and elastography methods have been collected and analyzed. The ultrasound method is based on ultrasound waves and is designed to examine the body's subcutaneous tissues and internal organs and their lesions. Ultrasound devices are widely available and have a more reasonable price than other devices (6, 7). Compared to other medical imaging techniques, they are safe, fast, non-invasive, painless, and relatively cheap (8).

Elastography is a non-invasive technique using ultrasound waves that measures the consistency of breast masses and enables doctors to make an early diagnosis without sampling (9). Elastography, in addition to the appearance and desired texture that conventional ultrasounds can detect, can show information about the hardness of the breast tissue and the distribution of the relative shape change (10). The location of a cancerous lesion in the breast is more prominent with elastography because an elastogram can also see tissues around the cancer. Elastography images increase diagnostic information due to the addition of information related to the elasticity of tissues. In elastography images, the elasticity of benign and malignant masses can be obtained and compared (11, 12). Elastography has been suggested as a complementary method for treatment. Elastography images are affected by movement, artifacts, and less contrast. Elastography is a non-invasive technique using ultrasound waves that measures the consistency of breast masses and enables doctors to make an early diagnosis without sampling. Elastography, in addition to the appearance and desired texture that conventional ultrasounds can detect, can show information about the hardness of the breast tissue and the distribution of the relative shape change (13). The location of a cancerous lesion in the breast is more prominent with elastography because an elastogram can also see tissues around the cancer. Elastography images increase diagnostic information due to the addition of information related to the elasticity of tissues (5). In elastography images, the elasticity of be-

* Corresponding author. Email: zhouyanjun2556@sina.com

nign and malignant masses can be obtained and compared (2). Elastography has been suggested as a complementary method for treatment. Elastography images are affected by movement, artifacts, and less contrast.

In a study by Vanithamani *et al*. (14), they proposed a new combined method to increase the visual quality of medical ultrasound images. Mammone *et al*. (15) showed that to improve ultrasound images, median filtering, local averaging, and compression with resampling (CRS) methods are used, and this algorithm is used in preprocessor computer-aided devices. In a study by Gómez-Flores *et al*. (16), to improve the elastography images and reduce the artifact, they used the ring method of artifact attenuation. To improve the ultrasound images, Menon *et al*. (17) used the speckle reduction anisotropic diffusion (SRAD) method and for segmentation using (seed point) and reached 93.89% accuracy. Xiao *et al*. (18) used the three steps of 3D boundary segmentation, feature extraction, and support vector machine (SVM) classifier to detect the mass in the 3D ultrasound of the breast and achieved a sensitivity of 90%. Five features of the elastographic mean (elasticity, maximum, standard deviation, degree of hardness, and extraction stretch ratio) and the optimal points of these five features were reported with the result of the area under the ROC curve, 91-98% and in it from (BI-RADS) is used to compare the diagnostic performance between black and white ultrasound and color SWE images (19).

In this research, the appropriate selection of the preprocessing method and the initial separation of the image textures from each other is an essential but very effective step. By selecting the image contrast enhancer and reducing the speckle noise with the improved method, we could use an enhanced-quality image in the segmentation stage. Two segmentation methods were evaluated, from which we found that the best channel can be selected using the characteristics of color channels. From the development of segmentation, we extract a self-similarity feature category. This feature has both shape features and quantitative information. Considering that most of the similar articles used the SVM network, in addition to this network, we used a set of neural networks and a combination of them to check the best network for the shape feature data extracted from the segmentation. For further evaluation, the Ki-67 protein cell proliferation index was also evaluated.

Materials and Methods

Data acquisition

A local database has been used to evaluate the efficiency of the proposed system. The data used in this article has been collected by a model ultrasound device (Mindray Resona7) respecting ethical issues. This data includes fourteen people with breast mass whose ultrasound and elastography images were recorded in BMP format.

Proposed method

The proposed method consists of three main stages:
1) Image preprocessing and processing
2) Feature extraction
3) Classification

Finally, the binary image output shows the healthy and lumpy areas. The appropriate method for each step has been selected using the test of different techniques and comparing the accuracy and precision performance evaluation criteria. Evaluating the effectiveness of the proposed method was also considered. Evaluation parameters include accuracy and precision. The definitions and calculation methods of each will be explained below.

Accuracy: the ratio of correct labels to the total labels given by the model that we have in Equation 1:

$$Accuracy\ (Ac) = \frac{TP\ +\ TN}{TP\ +\ FN\ +\ TN\ +\ FP}(\%) \quad [1]$$

Precision: the ratio of correctly recognized positive labels to the total number of positive labels of the model that we have in Equation 2:

$$\text{Precision (Pr)} = \frac{\mathbf{TP}}{\mathbf{TP + FP}}(\%) \quad [2]$$

Here, FP, TN, TP, and FN are equal to a false positive, true negative, true positive and false negative, respectively.

Pre-processing

Two preprocessing stages of histogram correction and preservation of inhomogeneous diffusion details (DPAD) have been used for preprocessing.

Histogram modification

The light intensity histogram of an image is the distribution of the light intensity of its discrete pixels. Adjusting the brightness of the image using the mapping of intensity values is called from the gray image to a new image. In this project, the brightness adjustment in the new image is such that 1% of the data goes to the minimum and maximum values of the gray level. This method increases the contrast of the image. The minimum and maximum values are chosen to cover less than and greater than 1% of all pixel values.

Maintenance heterogeneous release details

Xiao *et al*. (18) showed that preservation of inhomogeneous diffusion details was introduced, a method to reduce speckle noise without removing essential parts of the image. In other words, it is an improved filtering method (SRAD). The advantage of this method is that the improvement is made without removing a significant part of the content of the images, i.e., edges, lines, or other details that are important for the interpretation of the images. The equation of this model is shown in Equation 3.

$$I_p^{t+\Delta t} = I_p^t + \frac{\Delta t}{|\eta_p|} div\left[c\left(C_{p.t}\right)\nabla I_p^t\right] \quad [3]$$

I_p^t indicates the gray level, **t** the movement step, $|\eta_p|$ the number of pixels of the window, **p** the pixel location ∇I_p^t, and the value of the gray level gradient $(c_{p.t})$ indicate the ratio between the local deviation and the local average. Figure 1 shows two examples of pre-processed images using the DPAD method.

Normalized cutting method

Normalized cut (NC) is a graph segmentation problem based on a whole-image criterion for segmentation. The algorithm of this method defines a homogeneous patch for each pixel using the boundary map of the boundary detection function. It obtains this range's characteristic vectors of the intensity values (20).

First, we obtain the initial segmented image using

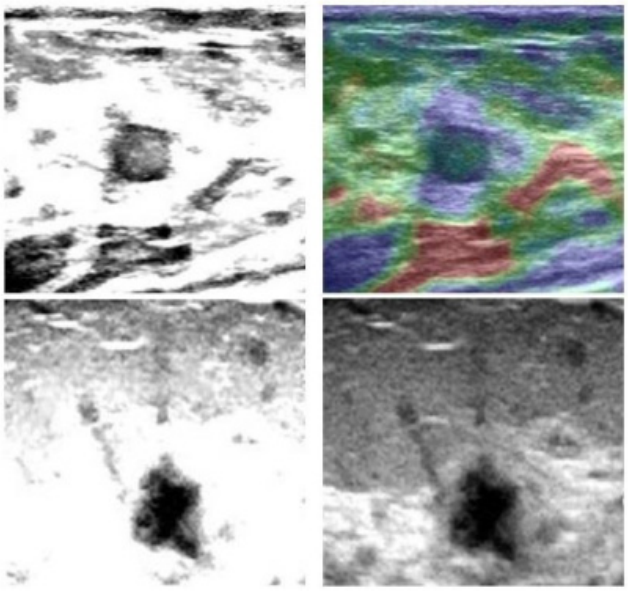

Figure 1. Two samples of elastography and ultrasound images (right images) and after pre-processing by DPAD method (left images).

thresholding. Then, using the obtained boundary results, we use the normalized cut segmentation method to improve the results. The effects of this method are enhanced by using k-means clustering to get the most significant region among other candidate regions in the whole image. We performed the segmentation test for ultrasound and elastography images.

Ki-67 protein cell proliferation index

The study was descriptive-analytical and cross-sectional, and simple random sampling was done from the archived blocks of patients with primary invasive ductal cancer in medical centers. Information related to the menopausal status of the patients was extracted from the files. From the samples molded in paraffin blocks by a microtome machine, 4-micron sections were prepared in 2 slides, one by the usual H&E method (hematoxylin and eosin) and the other by the Ki-67 kit with antibodies against the epitope of this antigen in the nucleus by the method Staining was similar to immunoperoxidase.

Before immunohistochemistry staining, on the slides stained with the H&E method, the area of the slide that had the least fibrosoncrosis and the most tumoral parenchyma was marked. On the other hand, the samples that were prepared from the tumor margin (due to higher mitotic activity) were selected. In this method, the tissue sections prepared on the slide were fixed with polylysine glue and stained in 5 steps, which were:

1. Hydrogen peroxidase stage
2. Primary antibody with negative control
3. Biotinylation step
4. Stritavidin stage
5. IIRP, substrate chromogenic product

The time of proximity of the sample with the target material was 10 minutes in each step, except for the first step, which should not last more than 5+1 minutes. Then, in each of the five mentioned steps, the slide was washed in water or buffer solution following the proximity with the cited materials, and after passing these steps, a counter stain was done.

With the help of slides stained with H&E, the histopathological grade was determined using the criteria in the IBlogn Richardson system in terms of nuclear pleomorphism, mitosis rate, and tubule formation. Thirty samples of each histopathological grade (III, II, I) were determined (in total, 90 samples). The percentage of cell proliferation index (Ki-67) was determined in the individual slides, and each sample was divided according to the positive percentage (Ki-67) into (low < 7%), (medium 8-12%), and (high > 12). Then, the average percentage of cell proliferation index (Ki-67) was determined in three groups related to the histopathological grade, and using the statistical facilities of analysis of variance, the relationship between cell proliferation index (Ki-67) and the prognostic factor of histopathological grade in invasive ductal breast cancers was determined. In this research, the menopause status was determined in 54 of the above samples and divided into two groups before and after menopause. The average percentage of cell proliferation index (Ki-67) in the two groups was determined using the Student t-test. Cell proliferation (Ki-67) and menopausal status were determined.

Results

The segmentation results of elastography images showed that the results of each image give a suitable answer according to pathological conditions or registration in one of the color channels. Figures 2 and 3 show segmentation results in green and red channels by elastography.

Feature extraction

The features used in this article are used for two purposes. The first goal is to separate the segmentation method created due to pathological and device characteristics. The second goal is to improve the accuracy and precision of the final segmentation. For the first purpose, we used the statistical features of each color channel. For the second purpose, because the shape was clear from the previous steps, the shape feature and intensity values were combined. Research shows that image histograms can be used as features. Texture metrics calculated using histo-

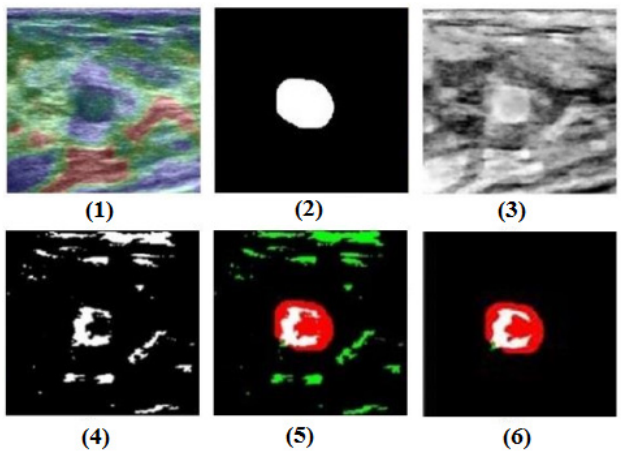

Figure 2. Review of the green channel, data number 8, original elastography image. [1], label determined by the doctor [2], pre-processed image [3], initial segmentation [4], comparison of segmentation with the label [5], and final output using the method (6 K-means). The green color is a false positive, the red color is a false negative, the black color is a true negative, and the white color is a true positive.

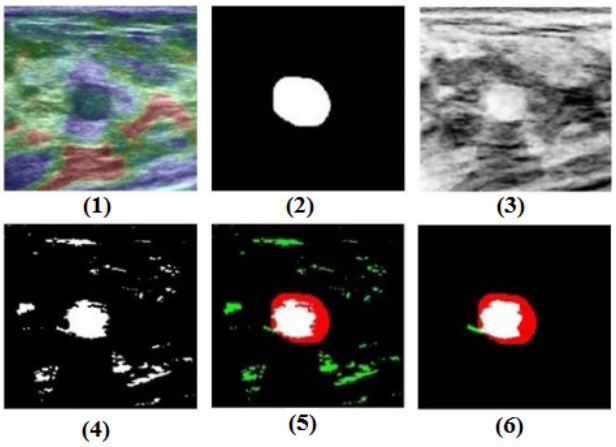

Figure 3. Comparison of data image number 8, in the red channel, the original elastography image. [1], the label determined by the doctor [2], the pre-processed image [3], the initial segmentation [4], the comparison of the segmentation with the label [5] and the final output using the K-means method [6]. The green color is a false positive. The red color is a false negative, the black color is a true negative, and the white color is a true positive.

grams have no information about the approximate position of pixels relative to each other. Accuracy and precision in different color channels are different from each other. Selecting the texture features of the channels makes it possible to achieve the resolution of the best color channel for the segmentation output. The average, standard deviation and entropy features were the primary statistical indicators chosen to describe the color elastography images. By normalizing these values between 0 and 1 and drawing them in the three-dimensional space, the resolution of each feature space was checked. We did. Variance (second torque) is particularly important in texture description. This torque is a measure of intensity contrast that can be used to create descriptors of relative texture smoothness. Standard deviation is also a measure of texture, which is more intuitive than variance. Entropy measures the randomness of elements. Table 1 shows the primary segmentation results based on accuracy and precision values in different color channels that are different from each other. Therefore, we assumed that we could achieve the resolution of the best color channel for the segmentation output based on the calculation of the texture features of the channels.

Figures 4 and 5 show some state results of the feature space. The feature space includes the standard deviation of all three channels (Figure 5), and the feature space consists of the entropy of all three channels (Figure 1). Figures 4 and 5 show that all three channels have linear separation conditions, as it is visible; we achieved 100% resolution of

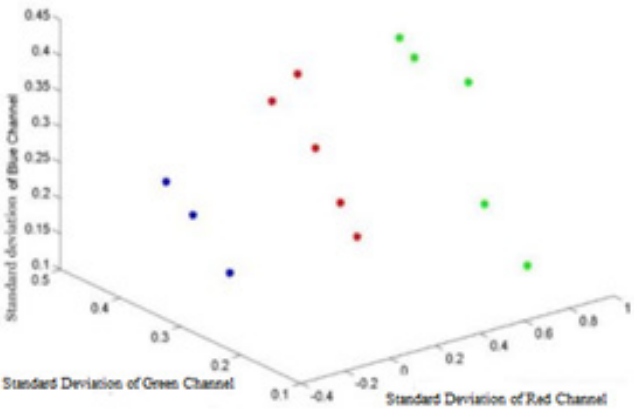

Figure 4. The standard deviation of the red channel, green channel and blue channel.

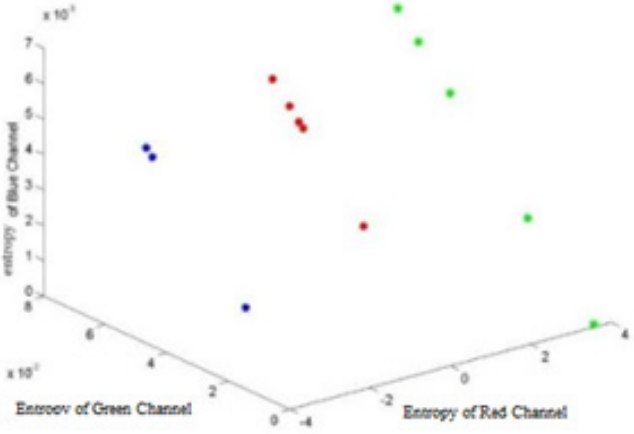

Figure 5. Red channel entropy, green channel entropy, and blue channel entropy

Table 1. Primary segmentation results in different color channels.

Data	Blue Channel		Green Channel		Red Channel	
	Precision	Accuracy	Precision	Accuracy	Precision	Accuracy
1	0.874	0	0.980	0.891	0	0.872
2	-	-	1	0.955	0.961	0.948
3	0.022	0.839	1	0.971	0.858	0.973
4	1	0.828	0.978	0.851	-	-
5	-	-	0.239	0.755	0.451	0.915
6	1	0.920	1	0.914	1	0.916
7	0.970	0.930	0	0.806	1	0.827
8	0	0.922	1	0.949	0.972	0.961
9	1	0.680	0	0.655	1	0.674
10	-	-	0	0.725	0.321	0.626
11	-	-	1	0.647	1	0.493
12	-	-	1	0.946	0.978	0.958
13	0	0.990	0	0.892	0.041	0.895
14	-	-	0.961	0.859	-	-

the best channel.

Shape feature

This method is such that for each pixel q, it produces a normalized correlation surface using small paths (d) and compares it with the larger environment of radius r. All three color channels are used for this feature and finally given to the classifier. We calculate these features for two regions of the segmentation output (first, for inside the mass and then for outside the mass). This work has been done by assuming the improvement of true positive increase and false positive decrease.

Comparison of ultrasound with elastography

After testing the segmentation results on elastography and determining the best channel to separate the mass from the tissue, the segmentation test is also performed on ultrasound. Table 2 compares ultrasound and elastography results based on accuracy and precision values.

The results show that ultrasound segmentation has six outliers out of 14. At the same time, elastography did not produce scattering data. In the remaining ultrasound results, the minimum and maximum accuracy is 56% and 98%, respectively, and the minimum and maximum accuracy is 98% and 100%, respectively. While in elastography, the average accuracy and precision are 92% and 97%. Due to separation in terms of color channels that contain the information load of tissue elasticity, elastography prevents data from being scattered and is chosen as a more appropriate method. We continue to process and improve segmentation with elastography images. Among the ultrasound and ultrasound data, there were some fundamental differences; these differences effectively justified the difference in the result of the comparison between these two types of images. In addition, it can be shown that according to the application, the use of each of these images has various information and applications. Figure 6 shows the comparison of elastography and ultrasound images.

Figure 7 shows that the ultrasound image label is different from elastography in terms of area. The larger area of the elastography image is due to the added information of this method.

As seen in Figure 7, the mass area in the elastography image is divided into two parts, which are considered the same area in ultrasound. In addition, the selection of elastography images compared to ultrasound is also clearly visible due to elastography segmentation. Due to the advantages of elastography images compared to ultrasound,

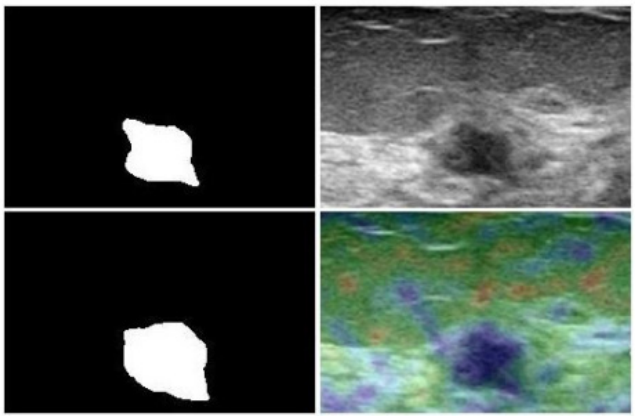

Figure 6. Image comparison of data Number 2; Ultrasound (top image, right), elastography (bottom image, right) and labels determined by the doctor (left images).

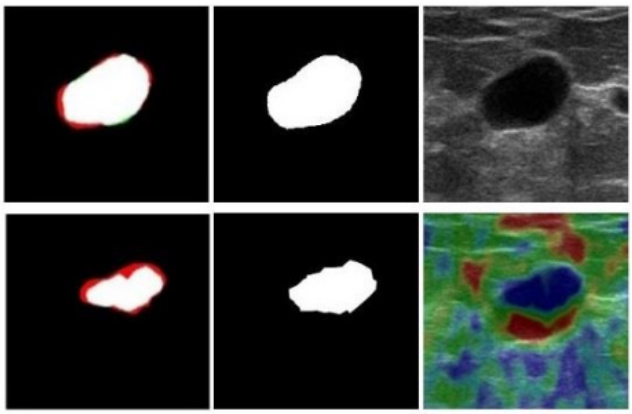

Figure 7. Comparison of data Number 3 between ultrasound (top), elastography (bottom) and labels determined by the doctor (middle), segmentation result (left).

Table 2. Comparison of ultrasound and elastography results.

Data	Selected color channel	Elastography		Ultrasound	
		Precision	Accuracy	Precision	Accuracy
1	Green	0.980	0.891	0.987	0.872
2	Green	1	0.955	-	-
3	Green	1	0.971	0.985	0.985
4	Green	0.978	0.851	-	-
5	Red	0.922	0.938	-	-
6	Blue	1	0.920	1	0.965
7	Blue	0.977	0.903	0.996	0.853
8	Red	0.972	0.961	0.997	0.966
9	Blue	1	0.680	-	-
10	Red	0.321	0.626	-	-
11	Red	1	0.493	1	0.560
12	Red	0.978	0.958	0.999	0.960
13	Green	1	0.928	1	0.918
14	Green	0.961	0.859	-	-

we continue to process and improve segmentation with elastography images.

Classification

The last step in the proposed method is the classification step, in which the feature matrix is entered into the classification algorithm. Then the labels determined by the algorithm are compared with those defined by the physician. In this article, different classification methods were used to show the system's efficiency, and the classification algorithms' results were evaluated and compared with each other to get the best result. We can mention support vector machines (SVM) and perceptron multilayer neural networks (K-means RBF MLP and SOM) from the tested algorithms.

The parameters used in the SVM network include the error stopping condition of 0.001, the number of repetitions of 10, the bias learning coefficient of 0.5, the training algorithm (BATCH), and the weight learning coefficient with the values of 0.1, 0.2, and 0.3. We found that good results are obtained for the learning coefficient of 0.3. We used the MLP network by changing the learning rate or alpha coefficient and the number of hidden neurons. We achieved linear input and output activity functions. Sigmoid tangent suppressed neuron activity function, error propagation network type, training algorithm (BATCH), number of selected hidden neurons 10, 70, 100, and alpha coefficient values 0.01, 0.02, and 0.03 by changing the number of hidden neurons, no significant improvement. The value of the results by changing the number of hidden neurons is almost equal. By examining the average execution time, it is suggested to use the number of hidden neurons to reduce the amount of computational processing and execution time. The required time is reduced with the lowest number of hidden neurons (10.37 ± 0.06 seconds). In RBF neural network, we used the Gaussian function and an inflation rate of 0.3. The initial value of random centers and training algorithm is (SEQUENTIAL). In the Kmeans network, the Euclidean distance method, number of clusters, random initialization (k), and training algorithm (BATCH) are used. In the SOM network, we used map dimensions of 10*15- 15*10- 5*5, and better results were obtained for map dimensions of 10*10.

Proposed hybrid networks

Support Vector Machines (SVM) are the most commonly used classifiers due to their excellent generalization performance. But SVMs are slower than neural networks in terms of execution time for multiple classification problems, and training them on a large dataset is still difficult. Although artificial neural networks are flexible and practical formats that can be applied to a wide range of predictive problems with high accuracy, they do not provide reliable answers in some cases, such as linear problems. Some researchers believe that linear models are better than artificial neural networks for linear problems that have linear relationships and do not have much disturbance. Therefore, blindly using artificial neural networks for all types of data is not smart. Using the combination of two methods as suitable strategies in real applications, including overcoming each model's limitations separately; Using each model's unique features. We propose a hybrid algorithm for training the RBF network based on K-means and SOM. This algorithm includes a proposed clustering algorithm to locate the RBF center and determine the least squares to calculate the weights. Also, MLP with scaled conjugate gradient (Graded Conjugate Scaled) has been used to show the comparison of different models based on experiments.

The MLP-SCG network is a multilayer perceptron neural network with a scaled conjugate gradient (SCG) that uses the numerical approximation of the matrix (Hessian) and avoids instability by combining the Levenberg-Marquardt algorithm with the scaled conjugate gradient method (21). It allows the scaled conjugate gradient to compute the training optimization to find the local minimum of the function without the need to perform the computationally expensive linear search, which is used by the traditional conjugate gradient algorithm (22).

RBF-SOM hybrid network

First, the training data is entered into the SOM, and the values of the centers are obtained using this network. The accepted centers are segmented by RBF Gaussian functions (22). Training algorithm (BATCH) and Gaussian neighborhood function were used.

RBF-KMEANS hybrid network

First, the training data is entered into k-means and using this network. The center values are obtained. The obtained centers are segmented by Gaussian RBF functions (21, 22). 20% of the data were considered for the training and 80% for the testing. To determine the classifier's accuracy, cross-validation, sometimes called circular estimation, has been used. Cross-validation is an evaluation method based on the classification results of the data set, which determines how generalizable and independent the training data is. In general, cross-validation involves dividing the data into two complementary subsets. The analysis is performed on one of those subsets (training data), and validation is performed using data from the other set (validation or test data). In order to reduce the dispersion, the validation process is performed several times with different divisions, and the validations' results are averaged. One of the standard methods in cross-validation is the K-Fold method. In this type of validation, the data is divided into K subsets. From these K subsets, each time, one is used for validation and another 1-n for training. This procedure is repeated K times, and all data are used precisely once for training and once for verification. The average result of these K validation times is reported as a final estimate. Of course, other methods can be used to combine the results.

General results

After evaluating different classification methods and comparing their results, the best classifier was proposed. The SVM network is removed from the desired networks due to having outlier data in both accuracy and precision evaluation. The RBF-SOM network is also removed from the optimal networks due to the negligible improvement of the result. The RBF-KMEANS network has increased the accuracy of all data, which has improved by at least 0.55 and at most 79.10%. There are two outlier data, and by removing them, the accuracy difference becomes 1729.1 + 2.0708. But the MLP-SCG network has improved the accuracy and precision of the results. (Increase in accuracy of 11 images out of 14, minimum improvement 82.3% and maximum 99.11%) considering that accuracy dispersion

Table 3. Comparing the results of different networks.

Method	Precision	Accuracy
MLP	0.8896	0.8575
MLP-SCG	0.9838	0.9436
RBF	0.8887	0.8449
K-mean	0.8391	0.8507
RBF-Kmeans	0.8937	0.8794
SOM	0.8783	0.8549
RBF-SOM	0.9230	0.8456
SVM	0.9000	0.8246

in 14 data is low (1.1726 ± 2.0708) and accuracy dispersion is high (7.0573 ± 3.5838).

We choose the MLP-SCG network as the proposed network. In Table 3, a comparison has been made between different networks. It should be noted that for the mentioned methods, the average precision and accuracy of the result have been shown in 16 cases. As can be seen, combined methods have better results compared to other methods. For example, the combination of k-means and RBF neural network has a noticeable improvement in accuracy compared to RBF or Kmeans alone. Also, the RBF-SOM method has better results than the SOM classifier by removing outlier data. The MLP-SCG method has performed better in terms of precision and accuracy than other methods.

Discussion

In this research, we used the idea of elastography images and the combined MLP-SCG network to identify masses. The results show that cancer diagnosis is highly dependent on the type of image and pathological characteristics, such as the percentage of the area occupied by the mass. Based on this, elastography images are more suitable than ultrasound. For each elastography data, the normalized cut (NC) method is performed on the best color channel, and by selecting the category of texture features of the channels, including mean, standard deviation, and entropy, and checking the shape features, it is possible to distinguish the best color channel for output segmentation achieved. The extracted feature categories were given to different networks for evaluation, among which the MLP-SCG neural network has improved significantly compared to other methods with an average accuracy of 94% and an average precision of 98%. This research has presented and evaluated a technique for detecting female breast cancer mass using elastography images and the combined MLP-SCG network to quickly improve the accuracy of diagnosis with a fast diagnosis and a new style (12).

Also, there is a significant difference between the average percentages of positivity (Ki-67 protein) in three groups with different histopathological grades, which was also confirmed in the statistical tests. The present research shows that the cell proliferation index (Ki-67 protein) has a significant relationship with the histopathological grade in invasive ductal breast cancer and that the histopathological grade is the most important prognostic factor previously confirmed in invasive ductal breast cancer (23).

The value of the cell proliferation index is determined as a factor in determining the prognosis. Previously, some studies have reported such a relationship for the cell proliferation index (Ki-67 protein) (24). To justify this phenomenon, the appearance of this Ki-67 protein in the nucleus of cells with high mitotic activity has been proposed. In contrast, tumoral cells without mitotic activity lack this protein (25). As a result, the cell proliferation index can be used in parallel with H&E staining in cases where it is impossible to accurately diagnose the microscopic histopathological grade and determine the prognosis in invasive ductal cancer. An increase in the percentage of positivity (Ki-67 index) can indicate a bad prognosis.

A previous study showed that average percentage of positivity of the cell proliferation index (Ki-67 protein) is related to the condition before and after menopause. Hence, breast cancer in young women before menopause often has a higher cell proliferation index (8). In the present study, the relationship between cell proliferation index (Ki-67 protein) and menopause status was significant. The present research shows that the cell proliferation index (Ki-67 protein) has a significant relationship with the histopathological grade in invasive ductal breast cancer and that the histopathological grade is the most important prognostic factor previously confirmed in invasive ductal breast cancer (26).

Besides, in the study by Xiao *et al*. (18), pre-processing steps, extraction of shape features (shape, form, and direction and textural features (echo pattern, border, and sound), segmentation, and classification are used. In (11) article, SVM was proposed to classify breast lesions in 3D ultrasound images, which reached a sensitivity of 97% and a specificity of 94%. Rodrigues *et al*. (27) illustrated that to improve the diagnosis of ultrasound images using the histogram balancing method, linear filtering (SRAD) and used a combination of these methods and used local area-based active counters method using SVM to segment the mass in breast ultrasound images and achieved an accuracy of 7.97%. In another study by Rodrigues *et al*. (28), to improve ultrasound images, they used the middle filter method and the histogram expansion to increase the contrast and the parametric active counter method to segment the images. In the article by Perona *et al*. (20), the histogram balancing method, fuzzy improvement, sigmoid-based improvement, and Watershed transform method were used to segment ultrasound images and achieved 80% accuracy. In the present study, considering the newness of the data used and the early detection of breast cancer by simultaneous use of ultrasound images and elastography, a method has been proposed which is very acceptable in terms of accuracy, sensitivity, and precision.

Acknowledgements
The authors are thankful to the higher authorities for the facilities provided.

Statements and Declarations
The author declares that no conflict of interest is associated with this study.

Authors' contribution
This study was done by the authors named in this article, and the authors accept all liabilities resulting from claims which relate to this article and its contents.

Conflicts of interest
There are no conflicts of interest.

Availability of data and materials

The data used to support the findings of this study are available from the corresponding author upon request.

Funding

The research was funded by Excellent Youth Talents Foundation of Traditional Chinese Medicine of Zhejiang Province (2021ZQ054).

References

1. Zoure AA, Bayala B, Bambara HA, Sawadogo AY, Ouedraogo C, Lobaccaro J A, Simpore J. Epidemiological Situation and Medical Management of Gynaecological and Breast Cancers from 1998 to 2018 in West Africa: A Systematic Review. Asian Pac J Cancer Biol 2020; 5(4): 211-219.
2. Zaker MR, Safaripour A, Sabegh SRZ, Barjasteh S. Supportive Intervention Challenges for Patients with Breast Cancer: A Systematic Review. Asian Pac J Enviro Cancer 2021; 4(1): 19-24.
3. Ahmed MS, Sayeed A, Mallick T, Syfuddin H. Knowledge and practices on breast cancer among Bangladeshi female university students: a cross-sectional study. Asian Pac J Cancer Care 2020; 5(1): 19-25.
4. Chakraborty A, Guha S, Chakraborty D. Micronutrients in preventing cancer: A Critical Review of Research. Asian Pac J Cancer Biol 2020; 5(3): 119-125.
5. Janbabaee G, Nadi-Ghara A, Afshari M et al. Forecasting the incidence of breast, colorectal and bladder cancers in north of Iran using time series models; Comparing Bayesian, ARIMA and Bootstrap Approaches. Asian Pac J Enviro Cancer 2021; 4(1): 3-7.
6. Olayide A, Isiaka A, Ganiyu R et al. Demographic pattern, tumor size and stage of breast cancer in africa: a meta-analysis. Asian Pac J Cancer Care 2021; 6(4): 477-492.
7. Aziziaram Z, Mattoo RU. A recombinant chimeric protein of protective antigen and lethal factor from Bacillus anthracis in polymeric nanocapsules showed a strong immune response in mice: a potential high efficacy vaccine against anthrax. Cell Mol Biol 2022; 68(3): 1-8.
8. Ogenyi SI, Onu JA, Ibeh NC, Madukwe JU, Onu OA, Menkiti FE. PIK3CA, KI67, Estrogen (ER) and Progesterone Receptors (PR) Expression Pattern of in HER2 Positive Breast Cancers. Asian Pac J Cancer Biol 2021; 6(4): 281-287.
9. Gubarkova EV, Sovetsky AA, Zaitsev VY et al. OCT-elastography-based optical biopsy for breast cancer delineation and express assessment of morphological/molecular subtypes. Biomed Opt Express 2019;10(5): 2244-2263.
10. Faiz M, Younus A, Yasmeen A. Genetic Diversity and Distribution of Vitamin D Receptor (VDR) Genotypes in Breast Cancer Cases from Pakistan. Asian Pac J Cancer Biol 2021; 6(4): 243-248.
11. Golmohammadi R, Mohajeri MR, Jarrahi AM, Moslem AR, Pejhan A. Histopathologic Characteristics of Invasive and Non-invasive Ductal Tumors have Relationship with Different Phenotypes of ER/PR Receptors in Breast Cancer Patients. Asian Pac J Cancer Biol 2021; 6(3): 181-185.
12. Park S-y, Kang BJ. Combination of shear-wave elastography with ultrasonography for detection of breast cancer and reduction of unnecessary biopsies: a systematic review and meta-analysis. Ultrasonography 2021; 40(3): 318.
13. Wu T-Y, Raghunathan V, Shi J, Hua W, Yu W, Deng A. Improving the outcomes of breast cancer in China: Physicians' Beliefs, Recommendations, and Practices for Breast Cancer Screening. Asian Pac J Cancer Care 2020; 5(4): 251-258.
14. Vanithamani R, Dhivya R, Sharmili S. A novel hybrid technique for visual enhancement of medical ultrasound images. IEEE International Conference on Computational Intelligence and Computing Research (ICCIC), 2015; 1-4.
15. Mammone R, Love S, Barinov L, Hulbert W, Jairaj A, Podilchuk C. Preprocessing for improved computer aided detection in medical ultrasound. IEEE Signal Processing in Medicine and Biology Symposium (SPMB), 2013;1-3.
16. Gomez-Flores W, Ruiz-Ortega BA. New fully automated method for segmentation of breast lesions on ultrasound based on texture analysis. Ultrasound Med Biol 2016; 42(7): 1637-1650.
17. Menon RV, Raha P, Kothari S, Chakraborty S, Chakrabarti I, Karim R. Automated detection and classification of mass from breast ultrasound images. Fifth National Conference on Computer Vision, Pattern Recognition, Image Processing and Graphics (NCVPRIPG), 2015; 1-4.
18. Xiao Y, Zeng J, Qian M, Zheng R, Zheng H. Quantitative analysis of peri-tumor tissue elasticity based on shear-wave elastography for breast tumor classification. Annu Int Conf IEEE Eng Med Biol Soc. 2013; 2013:1128-31.
19. Ye C, Vaidya V, Zhao F. Improved mass detection in 3D automated breast ultrasound using region based features and multi-view information. Annu Int Conf IEEE Eng Med Biol Soc 2014;2014:2865-8.
20. Perona P, Malik J. Scale-space and edge detection using anisotropic diffusion. IEEE Trans Pattern Anal Mach Intel 1990; 12(7): 629-639.
21. Shechtman E, Irani M. Matching local self-similarities across images and videos. IEEE Conference on Computer Vision and Pattern Recognition, 2007; 1-8.
22. Zhang B, Fu M, Yan H. A nonlinear neural network model of mixture of local principal component analysis: application to handwritten digits recognition. Pattern Rec 2001; 34(2): 203-214.
23. Zhou H, Zhao D. Ultrasound imaging-guided intracardiac injection to develop a mouse model of breast cancer brain metastases followed by longitudinal MRI. J Vis Exp 2014; (85): e51146.
24. Wu Q, Ma G, Deng Y, Luo W, Zhao Y, Li W, Zhou Q. Prognostic Value of Ki-67 in Patients With Resected Triple-Negative Breast Cancer: A Meta-Analysis. Front Oncol 2019; 9:1068.
25. Menon SS, Guruvayoorappan C, Sakthivel KM, Rasmi RR. Ki-67 protein as a tumour proliferation marker. Clinica chimica acta 2019; 491: 39-45.
26. Davey MG, Hynes SO, Kerin MJ, Miller N, Lowery AJ. Ki-67 as a prognostic biomarker in invasive breast cancer. Cancers 2021; 13(17): 4455.
27. Rodrigues PS, Giraldi GA, Provenzano M, Faria MD, Chang RF, Suri JS. A new methodology based on q-entropy for breast lesion classification in 3-D ultrasound images. Conf Proc IEEE Eng Med Biol Soc 2006;2006:1048-51.
28. Rodrigues R, Braz R, Pereira M, Moutinho J, Pinheiro AM. A two-step segmentation method for breast ultrasound masses based on multi-resolution analysis. Ultrasound Med Biol 2015; 41(6): 1737-1748.